

Variability of broad absorption lines in a QSO SDSS J022844.09+000217.0 on multi-year timescales

Zhi-Cheng He, Wei-Hao Bian*, Xiao-Lei Jiang & Yue-Feng Wang

Department of Physics and Institute of Theoretical Physics, Nanjing Normal University, Nanjing 210023, China

12 June 2021

ABSTRACT

The variability of the broad absorption lines is investigated for a broad absorption line (BAL) QSO, SDSS J022844.09+000217.0 ($z = 2.719$), with 18 SDSS/BOSS spectra covering 4128 days in the observed frame. With the ratio of the rms spectrum to the mean spectrum, the relative flux change of the BAL-trough is larger than that of the emission lines and the continuum. Fitting the power-law continuum and the emission line profiles of C IV $\lambda 1549$ and Si IV $\lambda 1399$, we calculate the equivalent width (EW) for different epochs, as well as the continuum luminosity and the spectral index. It is found that there is a strong correlation between the BAL-trough EW and the spectral index, and a weak negative correlation between the BAL-trough EW and the continuum luminosity. The strong correlation between the BAL-trough EW and the spectral index for this one QSO suggests that dust is intrinsic to outflows. The weak correlation between the BAL variability and the continuum luminosity for this one QSO implies that the BAL-trough variation is not dominated by photoionization.

Key words: galaxies:active—galaxies:nuclei—quasars:absorption lines

1 INTRODUCTION

Broad absorption line quasars (BAL QSOs) exhibit broad, ultraviolet (UV) line absorption troughs. The traditional BAL QSOs were quantified by balnicity index (BI) with velocity width larger than 2000 km s^{-1} and outflow velocity of $3000\text{--}25000 \text{ km s}^{-1}$ (Weymann 1991). There are a large number of broad absorption features within 3000 km s^{-1} and beyond 25000 km s^{-1} , as well as features with widths less than 2000 km s^{-1} , and newer ways of quantifying the index (e.g. Hall et al. 2002; Trump et al. 2006; Gibson et al. 2009). BAL troughs are present in about 10–40% of QSOs (e.g. Hewett & Foltz 2003; Trump et al. 2006; Ganguly et al. 2007; Allen et al. 2011), produced by absorption from high-ionization lines such as Si IV $\lambda 1399$, C IV $\lambda 1549$, C III] $\lambda 1909$ (known as HiBAL), and low-ionization lines such as Mg II $\lambda 2799$ (known as LoBAL). The fraction of BAL QSOs strongly depends on the definition of BAL QSOs (e.g. Hewett & Foltz 2003; Trump et al. 2006), so drawing physical conclusions from population statistics must be done with care.

BAL troughs are thought to be the strongest observed signatures of QSO winds (Fabian 2012). The observation of BALs is commonly thought to be the result of passing a disk wind along the line of sight (e.g. Murray et al. 1995; Elvis

2000). If the wind is on the line of sight, a QSO appears as a BAL QSO. That detection of a wind should be orientation-dependent is very similar to the case of other structures in QSOs, such as the broad line region (BLR) or jet (e.g. Urry & Padovani 1995).

However, it was found that there is no significant difference between radio spectral index distributions for radio-loud BALs and radio-loud non-BALs, indicating they have similar ranges of viewing angles (Becker et al. 2000; Montenegro-Montes et al. 2008; Fine et al. 2011; Bruni et al. 2012). No correlations exist between outflow properties and the orientation, suggesting that BAL winds along any line of sight are driven by the same mechanisms (DiPompeo et al. 2012). There are also BAL QSOs that are seen very nearly along the radio jet axis (Zhou et al. 2006; Ghosh & Punnsly 2007). Another explanation for BALs is an orientation-independent evolution effect (e.g. Gibson et al. 2008; Zubovas & King 2013). BALs outflow is possibly caused by the expulsion of gas and dust by galaxy collision as an evolutionary stage of AGN (e.g. Voit et al. 1993; Gregg et al. 2006; Gibson et al. 2008).

The disk wind is believed to come from the central accretion disk in QSOs (e.g. Murray et al. 1995). The dependence of wind properties (such as the trough EW, the maximum velocity, the fraction of BAL QSOs) on the physical properties of QSOs (such as the luminosity, the He II $\lambda 1640 \text{ \AA}$ EW, and the UV continuum slope) has been inves-

* E-mail: whbian@njnu.edu.cn

tigated by many authors, and they found some correlations between them (Laor & Brandt 2002; Ganguly et al. 2007; Baskin et al. 2013). It was found that the maximum outflow velocities increase with both the bolometric luminosity and the blueness of the spectral slope, suggesting the idea of radiation pressure-driven outflows (Laor & Brandt 2002; Ganguly et al. 2007).

BAL troughs often vary in equivalent width (EW) and/or shape over rest-frame timescales of months to years (e.g. Barlow et al. 1992; Gibson et al. 2008; Filiz Ak et al. 2012, 2013). It was found that the fractional EW change increases with rest-frame timescale over the range 0.05 - 5 yr (e.g. Gibson et al. 2008; Filiz Ak et al. 2013). The BAL-trough variation is believed to be driven by changes in velocity structure, covering factor, or ionization level (e.g. Filiz Ak et al. 2012). It was suggested that BAL variation arises from changes in the amount of "shielding gas" along the line-of-sight (Filiz Ak et al. 2013). Such changes are likely according to disk-wind simulations (e.g. Proga et al. 2000; Murray et al. 1995). These changes could ultimately be related to the central accretion disk (e.g. Proga et al. 2000). Changes in the column density of shielding gas (BAL trough EW variability) can relate to the level of ionizing luminosity reaching the BAL wind.

Two kinds of investigations of BAL-trough variability have typically been undertaken. One is to use two-epoch spectra in a BAL sample; the other is to use multi-epoch spectra for one single object (e.g. Gibson et al. 2008; Filiz Ak et al. 2013; Capellupo et al. 2011, 2012, 2013). Using a two-epoch sample of 13 BAL QSOs overlapping between the Very Large Array (VLA) Faint Images of the Radio Sky at Twenty-Centimeter (FIRST) Survey and the Sloan Digital Sky Survey (SDSS), Gibson et al. (2008) found that BALs tend to vary on multi-year timescales in velocity regions that are a few thousand kilometers per second wide. They also found that BAL-trough variations do not appear to be correlated with variations in the observable continuum, implying that the BAL-trough variation is not dominated by photoionization changes (e.g. Barlow et al. 1989; Capellupo et al. 2012). Capellupo et al. (2011, 2012, 2013) did extensive variability studies on a small BAL QSO sample with longer timescales and multiple epochs. They found that the variability occurs typically in only portions of the BAL troughs; the components at higher outflow velocities are more likely to vary than those at lower velocities, and weaker BALs are more likely to vary than stronger BALs. The shortest timescales constrain the location of the outflowing gas. With a larger SDSS sample, Filiz Ak et al. (2013) found that there is a relation between the luminosity and EW variability on moderate timescales, although they did not regard this case as strong evidence for luminosity dependence.

The BAL-trough variability for one single object is very important in understanding of the origin of the BAL QSOs. With the SDSS, a large number of BAL QSOs are found in various data releases (e.g. Trump et al. 2006; Gibson et al. 2009; Shen et al. 2011; Paris et al. 2013). We selected a single QSO, SDSS J022844.09+000217.0, which has the highest number of observations in the time domain, to investigate the relation between the wind and QSO properties. §2 presents the data. §3 gives the data analysis. §4 contains our results and discussion. The Summary is given in the

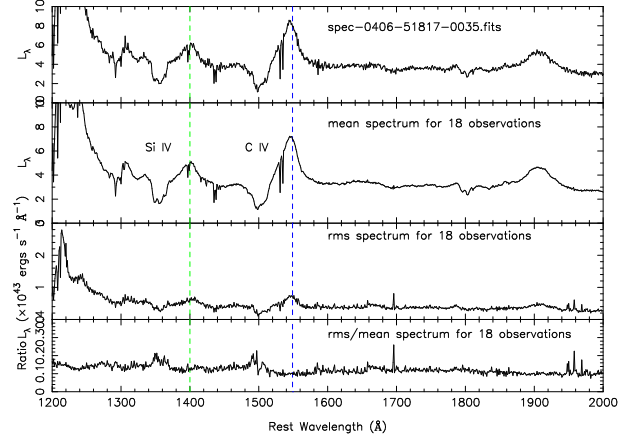


Figure 1. A typical single spectrum (top panel), the average spectrum (second panel), the root-mean-square (rms) spectrum (third panel), the ratio of the rms spectrum to the average spectrum (i.e., the relative flux change, bottom panel) from total 18 spectra for SDSS J022844.09+000217.0. The dotted lines show the wavelengths of Si IV λ 1400 Å and C IV λ 1549 Å.

last section. Throughout this work we use a cosmology with $H_0 = 70 \text{ km s}^{-1} \text{ Mpc}^{-1}$, $\Omega_M = 0.3$, and $\Omega_\Lambda = 0.7$.

2 SDSS/BOSS SPECTRAL DATA

The Baryon Oscillation Spectroscopic Survey (BOSS), part of SDSS-III, uses the dedicated 2.5-m wide-field telescope at Apache Point Observatory near Sacramento Peak in Southern New Mexico to conduct an imaging and spectroscopic survey for about 1.5 million luminous galaxies as well as about 160,000 quasars at $z > 2.2$ (Eisenstein et al. 2011). With respect to the original SDSS, the wavelength coverage of BOSS spectra changes from 3800 Å - 9200 Å to 3600 Å - 10400 Å, as well as the fiber numbers per plate from 640 to 1000. And the BOSS uses new fibers (1000 rather than 640 per plate), with smaller holes (2" rather than 3").

With SDSS DR7, Shen et al. (2011) gave a compilation of properties of the 105783 QSOs. There are 6214 BAL QSOs in their SDSS DR7 sample (see also Gibson et al. 2009). There are 456 C IV BAL QSOs with at least two-epoch spectroscopic observations. We searched for observations of these 456 C IV BAL QSOs in SDSS DR10 and found more epochs of spectroscopy for each object. The one BAL QSO with the most observations, SDSS J022844.09+000217.0 ($z = 2.719$), has 18 high signal-to-noise ratio (S/N) SDSS/BOSS spectra, covering 4128 days (about 11 years) in the observed frame (Table 1), i.e., about 3 years in the rest frame. For SDSS spectra, the S/N in the r-band is about 17-20. The BOSS spectra have longer exposure times than the SDSS sample, and have a better S/N about 22-36. In Table 1, the information for these 18 spectra is listed, such as the survey name, MJD, Plate, Fiber ID, S/N.

Table 1. The properties of 18-epoch spectra for SDSS J022844.09+000217.0. Col(6-9): in units of Å. Col(10): measured from 1300Å to 2400Å, in units of $10^{43} \text{ erg s}^{-1} \text{ Å}^{-1}$. Col(12): in units of km s^{-1} . EW_1 is measured based on a power-law continuum. EW_2 is measured based on a pseudo-continuum of power-law continuum plus emission lines.

Survey (1)	MJD (2)	Plate (3)	Fiber (4)	SN(r) (5)	$EW_1(\text{C IV})$ (6)	$EW_2(\text{C IV})$ (7)	$EW_1(\text{Si IV})$ (8)	$EW_2(\text{Si IV})$ (9)	L_{cont} (10)	α (11)	V_{max} (12)
SDSS	51817	406	35	17.1	12.86 ± 0.79	18.14 ± 1.23	8.59 ± 0.55	9.48 ± 0.62	3.69 ± 0.16	-0.76 ± 0.02	12738
SDSS	51869	406	37	19.6	15.33 ± 0.91	19.32 ± 1.12	9.77 ± 0.49	10.66 ± 0.54	3.20 ± 0.13	-1.16 ± 0.03	13124
SDSS	51876	406	37	17.0	14.35 ± 1.01	18.13 ± 1.24	8.90 ± 0.58	10.26 ± 0.67	3.50 ± 0.15	-0.79 ± 0.03	12738
SDSS	51900	406	36	17.0	14.96 ± 0.80	19.58 ± 1.32	9.29 ± 0.57	10.08 ± 0.63	3.72 ± 0.17	-0.74 ± 0.03	12738
SDSS	52200	705	431	15.6	15.62 ± 1.21	20.07 ± 1.52	9.23 ± 0.63	10.29 ± 0.70	2.99 ± 0.16	-0.75 ± 0.03	13317
SDSS	52205	704	640	16.6	16.00 ± 1.03	19.57 ± 1.35	8.93 ± 0.52	9.64 ± 0.57	2.94 ± 0.16	-0.90 ± 0.03	13124
SDSS	52238	406	39	19.3	16.70 ± 1.11	20.55 ± 1.35	9.20 ± 0.62	9.82 ± 0.67	3.59 ± 0.13	-0.77 ± 0.03	13703
BOSS	55179	3615	780	36.6	17.02 ± 0.54	22.67 ± 0.71	10.97 ± 0.31	12.32 ± 0.35	3.03 ± 0.07	-0.32 ± 0.02	13703
BOSS	55181	3647	778	28.6	16.10 ± 0.67	22.33 ± 0.91	10.16 ± 0.38	11.33 ± 0.43	3.16 ± 0.09	-0.32 ± 0.02	13703
BOSS	55208	3615	780	29.0	16.24 ± 0.59	21.60 ± 0.77	10.18 ± 0.34	11.16 ± 0.38	2.67 ± 0.07	-0.67 ± 0.02	13703
BOSS	55209	3744	575	22.3	15.15 ± 0.83	20.35 ± 1.10	10.08 ± 0.51	11.03 ± 0.49	2.90 ± 0.09	-0.62 ± 0.03	13896
BOSS	55241	3647	778	33.8	16.46 ± 0.57	22.56 ± 0.77	10.33 ± 0.33	11.47 ± 0.35	3.19 ± 0.07	-0.46 ± 0.02	14089
BOSS	55445	3615	770	27.7	15.94 ± 0.73	21.61 ± 0.97	9.97 ± 0.41	11.17 ± 0.36	2.87 ± 0.09	-0.41 ± 0.02	14089
BOSS	55455	4238	736	30.8	16.40 ± 0.63	22.09 ± 0.83	9.56 ± 0.32	10.50 ± 0.42	3.13 ± 0.09	-0.73 ± 0.02	14089
BOSS	55476	3647	786	34.0	16.58 ± 0.59	22.54 ± 0.78	10.34 ± 0.32	11.49 ± 0.40	3.43 ± 0.09	-0.54 ± 0.02	13896
BOSS	55827	3647	780	37.0	17.69 ± 0.67	22.80 ± 0.86	10.86 ± 0.38	12.07 ± 0.43	3.22 ± 0.10	-0.62 ± 0.02	14089
BOSS	55856	3615	776	32.5	17.83 ± 0.80	22.94 ± 1.04	11.27 ± 0.44	12.74 ± 0.50	3.16 ± 0.12	-0.40 ± 0.02	14089
BOSS	55945	3647	738	35.4	16.11 ± 0.65	22.14 ± 0.90	10.67 ± 0.40	11.95 ± 0.45	3.53 ± 0.12	-0.44 ± 0.02	13896

Table 2. Summary of the Spearman correlation coefficients: EW_1 is measured based on a power-law continuum. EW_2 is measured based on a pseudo-continuum of a power-law continuum plus emission lines. EW_h is measured within the high-velocity part. EW_l is measured within the low-velocity part. The first two lines are for the C IV BAL-trough, and the last two lines are for the Si IV BAL-trough. The value in brackets is the probability of the null hypothesis. L_{cont} is measured from 1300Å to 2400Å.

		EW_1	EW_2	EW_h	EW_l
C IV	L_{cont}	-0.19 (0.443)	-0.21 (0.399)	-0.22 (0.39)	-0.28 (0.26)
	α	0.45 (0.06)	0.77 (0.00018)	0.64 (0.0042)	0.87 (0.000003)
Si IV	L_{cont}	-0.24 (0.33)	-0.22 (0.37)	-0.35 (0.15)	-0.22 (0.39)
	α	0.78 (0.00013)	0.81 (0.00004)	0.75 (0.0003)	0.82 (0.00003)

3 ANALYSIS

3.1 Mean and RMS spectra

The mean spectrum from these 18 spectra is calculated as follows:

$$f_{mean}(\lambda) = \sum_{i=1}^N \frac{f_i(\lambda)}{N}$$

where the sum is taken over the $N = 18$ spectra. From the mean spectrum with high S/N, the absorption region and emission region are more obvious, which can help us choose suitable continuum windows. The root-mean-square (rms) spectrum from the 18 spectra is determined by:

$$f_{rms}(\lambda) = \left\{ \frac{1}{N-1} \sum_{i=1}^N [f_i(\lambda) - f_{mean}(\lambda)]^2 \right\}^{1/2}$$

where the sum is taken over the $N = 18$ spectra (e.g., Kaspi et al. 1999). For the spectrum at MJD = 52205, the data from 1660 Å – 1798 Å (rest wavelength) are not used. The mean spectrum and the rms spectrum are shown in Fig. 1., as well as a single spectrum (top panel).

From the mean spectrum (second panel in Fig. 1), the

broad absorption troughs in Si IV and C IV are obvious, as well as some narrow absorption lines. From the rms spectrum, the emission region varied significantly larger than the absorption region (third panel in Fig. 1). The rms-to-mean ratio spectrum, i.e., the relative flux change, is shown in the bottom panel of Fig. 1. The variance fraction from these 18 spectra increases as the frequency increases, from about 10% on the red side to about 15% on the blue side. The relative flux change is larger for the absorption trough than for the continuum and the emission lines.

In Fig. 2, we also show all 18 spectra normalized at 2000 Å. There is clear variability of the spectral slope during this long timescale of about 11 years.

3.2 Fitting the spectrum

In order to investigate the relation between the BAL-trough and QSO properties, we fit the continuum and the emission line profiles as follows (Hu et al. 2008; Zhang et al. 2010; Bian et al. 2012; Capellupo et al. 2012):

(1) Fitting the continuum. All the observed spectra are corrected for Galactic extinction using an A_V value of 0.1575, assuming the extinction curve of Cardelli et al.

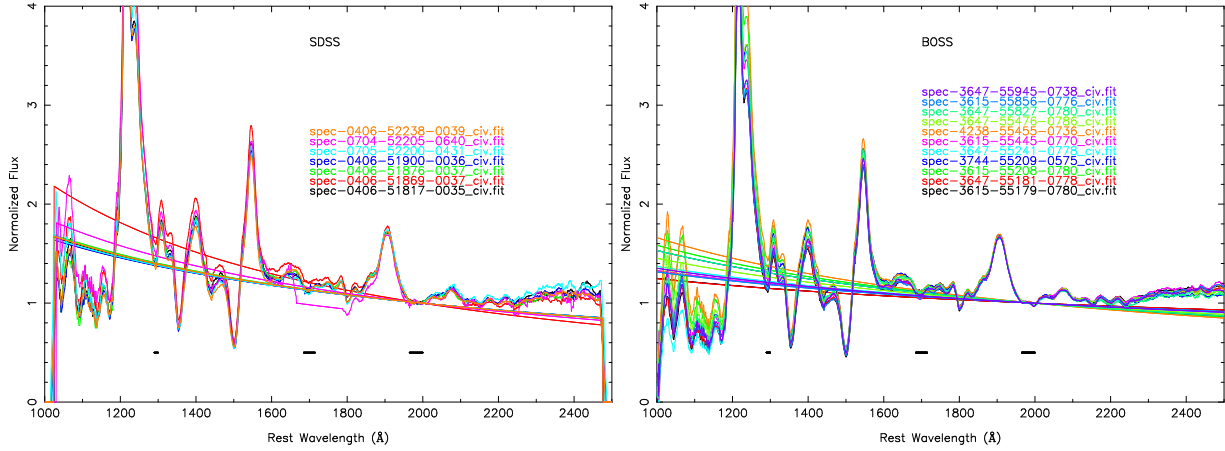


Figure 2. All 7 SDSS (left) and 11 BOSS (right) spectra normalized at 2000 Å with a smoothing box of 20 Å. The power-law continuum is plotted in this figure. The black horizontal lines are the continuum windows for the power-law fit.

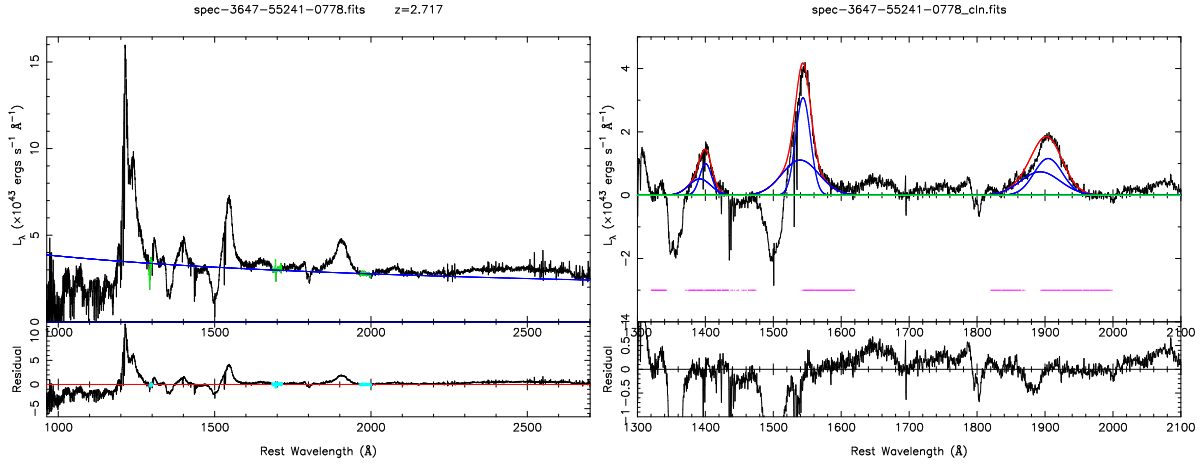


Figure 3. An example of the power-law continuum fit (left) and the emission line fit (right). Left top: The extinction-corrected rest-frame spectrum is shown by the black lines. The green dots are the initial continuum windows. The blue line is the power-law continuum. Left bottom: the residual spectrum. Right top: The multiple Gaussian components are in blue and the sum of these is in red. The fitting window is in blue. The horizontal pink dots are the final data used in emission line fit. Right bottom: the residual spectrum.

(1989; IR band; UV band) and O'Donnell (1994; optical band) with $R_V = 3.1$. And they are converted to the rest frame by redshift of $z = 2.717$. It is common to use the power-law formula, $f_\lambda \propto \lambda^\alpha$ ($f_\nu \propto \nu^{-(2+\alpha)}$) to approximately fit the QSO continuum spectrum. Other continuum models, such as a polynomial function or a reddened power-law, have also been used in previous studies (Lundgren et al. 2007; Gibson et al. 2009). We fit the power-law continuum iteratively in the "continuum windows", which are known to be relatively free from strong emission lines. The fit is performed by minimizing χ^2 . From Fig. 1, we select the following continuum windows: 1290-1300, 1685-1715, 1965-2000 Å in the rest frame (e.g. Forster et al. 2011; Vanden Berk et al. 2001; Gibson et al. 2008; Bian et al. 2012; Baskin et al. 2013). At each iteration, we ignore any spectral bins that deviate by more than 3σ from the previous iteration's continuum fit. That iterative approach would exclude additional spectral regions that contain broad emission or absorption features, especially for BAL QSOs. For this object, we don't fit the UV Fe II emission. The power-law continuum is also shown in Fig. 3. An

example of the continuum fit and the residual is shown in the left panel of Fig. 3.

(2) Fitting the broad emission lines. Considering the broad wing in the broad emission line profiles, we use three sets of two Gaussians to simultaneously model emission line profiles for Si IV λ 1399, C IV λ 1549, C III] λ 1909 in the continuum-subtracted spectra. Each emission line is fit iteratively. At each iteration, the "absorbed" bins are ignored when they are more than 2.5σ below the previous model fit. In order to eliminate absorption trough impact on the fitting of the emission lines of the C IV, Si IV, C III], especially in the blue wings of these lines, the fitted weights of the blue wings for these emission lines are set to half of normal. And the weights of the red wings are set to twice normal. An example of the line fit and the residual is shown in the right panel of Fig. 3. The horizontal pink dots are for the line fitting. The red lines show the sum of the blue Gaussian profiles for the different lines.

3.3 The BAL EW and the maximum velocity of outflow

Two methods are used to calculate the BAL-trough EW. One is based on the power-law continuum, the other is based on the pseudo-continuum of the power-law plus the emission lines. The latter includes the BAL correction from the emission lines. The equivalent widths of the BAL-troughs for Si IV and C IV are calculated as follows:

$$EW = \int [1 - \frac{f_{obv}(\lambda)}{f_{con}(\lambda)}] d\lambda$$

The integration is done for $f_{obv}(\lambda) < f_{con}(\lambda)$. From Fig. 5, for the Si IV λ 1399 BAL, its EW is integrated from 1340 Å to 1400 Å, and for the C IV λ 1549 BAL, its EW is integrated from 1450 Å to 1550 Å. The EW results are shown in Cols. 6-9 in Table 1, where the subscript of 1 is for the case based on the power-law continuum (EW_1), and the subscript of 2 is for the case based on the pseudo-continuum of the power-law plus the emission lines (EW_2). The latter EW is larger than the former one. The EW_2 are about 10% larger than the EW_1 for Si IV, while the difference is about 25% for C IV.

We also measure the maximum velocity of outflow. We searched each spectrum for absorption troughs at a level of 10% below the continuum as given in the traditional definition of a BAL. The maximum velocity corresponds to the shortest wavelength for a given trough with at least 10 Å deeper than 10% below the continuum. The result is listed in Col. (12) in Table 1.

For the power-law continuum, $f_\lambda = f_{2000}(\lambda/2000\text{Å})^\alpha$, the error for the power-law continuum at the wavelength of λ by error propagation is:

$$\delta(f_{con}) = f_\lambda \sqrt{(\frac{\delta(f_{2000})}{f_{2000}})^2 + (\ln \lambda - \ln 2000)^2 \delta\alpha^2}$$

where the errors of $\delta(f_{2000})$ and $\delta\alpha$ are given in the power-law fitting. The error for the BAL EW is measured as follows:

$$\delta(EW) = \sqrt{\sum_{\lambda} (\frac{f_{obv}}{f_{con}})^2 [(\frac{\delta(f_{obv})}{f_{obs}})^2 + (\frac{\delta(f_{con})}{f_{con}})^2]}$$

where $\delta(f_{obv})$ at λ is the error in the SDSS/BOSS spectrum.

4 RESULTS AND DISCUSSION

4.1 Relation between the C IV emission line luminosity and the continuum

There is a correlation between the C IV luminosity and the continuum, where the continuum is the mean power-law luminosity between 1300 Å and 2200 Å. The Spearman coefficient R is 0.67 with the probability of the null hypothesis of $P_{null} = 0.002$. It is consistent with the photoionization scenario and classic Baldwin effect for the emission lines in QSOs.

4.2 The light curves for BAL-trough C IV EW

Fig. 4 gives the light curves of C IV EW, as well as the continuum, and the spectral index α (from top to bottom panel).

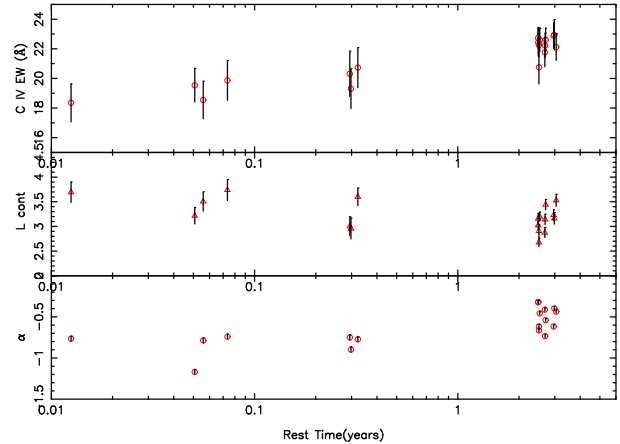


Figure 4. The light curves for C IV BAL EW, the continuum (measured from 1300 Å to 2400 Å) and α . The continuum is in units of $10^{43}\text{erg s}^{-1}\text{Å}^{-1}$.

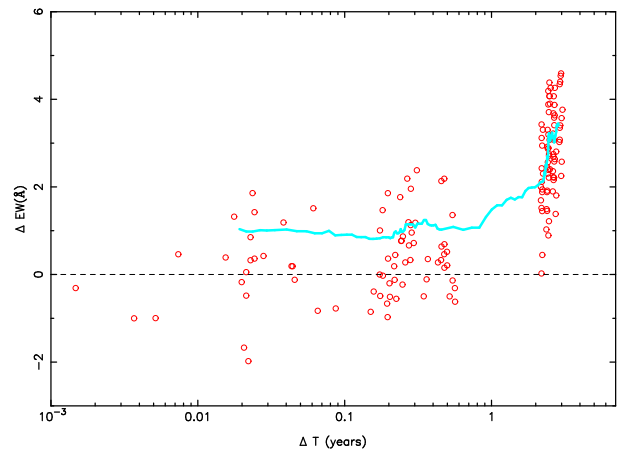


Figure 5. C IV BAL EW variation versus timescale for two-epoch spectra in the rest frame. The cyan line is the standard deviation derived from the data, calculated using a sliding window containing 20 time-ordered data points. The standard deviation of EW variation increases with increasing rest-frame timescale.

The shortest time interval is one day, and the longest time interval is about 11 years in the observed frame. With time, there is an increasing trend of C IV EW and the spectral index, and a decreasing trend of the continuum. The largest EW changes are about 25% (from 18.1 Å to 22.7 Å) for C IV and 28% (from 8.6 Å to 11.0 Å) for Si IV.

It was found that C IV BAL-trough variability is larger for longer timescales (e.g. Gibson et al. 2008; Capellupo et al. 2012; Filiz Ak et al. 2013). We also give the EW variation versus the time interval for two-epoch spectra (Figure 5). For longer time intervals, the EW variation is larger for this object. That result is consistent with previous studies (e.g. Filiz Ak et al. 2013).

We also find that there is a strong correlation between the C IV BAL-trough EW and the Si IV BAL-trough EW. The Spearman correlation coefficient is 0.7 ($P_{null} = 0.003$) for EW_1 and 0.8 ($P_{null} = 7 \times 10^{-6}$) for EW_2 .

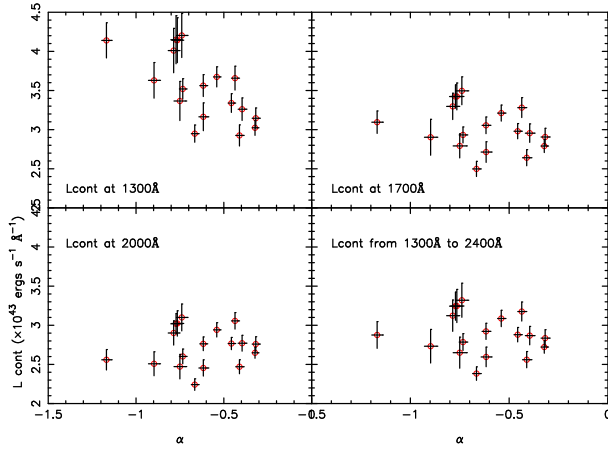


Figure 6. The continuum versus the spectral index α . The continuum is measured at 1300 Å (left top), at 1700 Å (right top), at 2000 Å (left bottom), and from 1300 Å to 2400 Å (right bottom). The correlation becomes stronger when the continuum luminosity is measured for the bluer bands.

4.3 The continuum versus the spectral index α

For the slope variation in QSOs, some investigations found that spectra of QSOs with low redshift are bluer during their brighter phases (e.g. Vanden Berk et al. 2001; Pu 2006). However, with two-epoch variation, it was recently found that the spectra of half of the QSOs appear redder during their brighter phases, especially for high- z QSOs (Bian et al. 2012). From Fig. 1, we find that the variability is larger for the blue side in the rms or rms/mean spectra. The slope α changes about 260% (from -0.32 to -1.16, Table 1). In Fig. 6, we show the relation between the continuum and α . In order to avoid accidental conclusions, we measured four different continuum luminosities from the mean power-law luminosity at different monochromatic wavelengths or wavelength interval: (1) 1300 Å to 2400 Å; (2) 1300 Å; (3) 1700 Å; (4) 2000 Å. The continuum luminosity (from 1300 Å to 2400 Å) changed by about 38%. The Spearman correlation coefficients between the continuum luminosity and α are -0.69 (0.001), -0.36 (0.14), -0.001 (0.997), -0.30 (0.23) (from top to bottom and from left to right in Fig. 6), where the values in brackets are the probabilities of the null hypothesis. The correlation becomes stronger when the continuum luminosity is measured for the bluer bands. This correlation shows that this QSO has a steeper UV slope when its luminosity increases. This kind of negative correlation is consistent with some previous studies for PG QSOs (e.g. Pu 2006).

4.4 EW versus the spectral index α

Fig. 7 displays the relation between the BAL-trough EW and the spectral index α for C IV (top) and Si IV (bottom). The blue squares denote the EW_1 data, i.e., based on the power-law continuum. Red circles denote the EW_2 data, i.e., based on the pseudo-continuum of the power-law plus the emission lines. Due to the correction of the emission lines, the value of EW_2 is larger than EW_1 . The correlation between the EW and α is strong. The correlation coefficient is 0.45 (0.06) for C IV EW_1 , 0.77 (0.00018) for C IV EW_2 , 0.78 (0.00013) for Si IV EW_1 , and 0.81 (0.00008) for Si IV EW_2 , where the values in brackets are the probabilities of the null hypothesis.

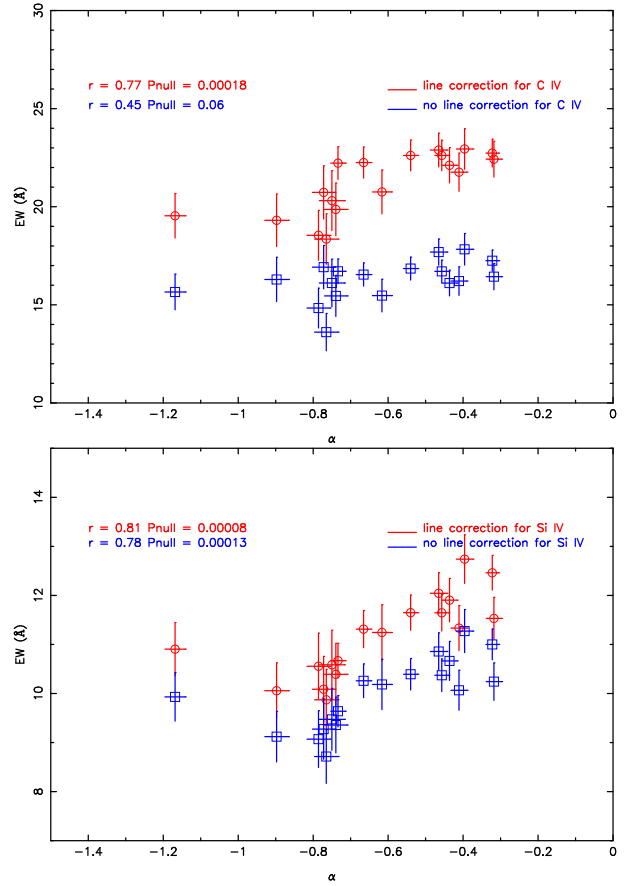


Figure 7. The BAL-trough EW versus spectral index α for the C IV BAL (top), and for the Si IV BAL (bottom). The blue square is for the case based on the power-law continuum fit. The red circle is for the case based on the pseudo-continuum fit of the power-law plus the emission lines.

With the correction from the emission lines creating deeper troughs, stronger correlations are found for the C IV and Si IV BAL-troughs. We list these correlation coefficients in Table 2.

This result shows that the BAL-trough EW becomes larger when the UV slope becomes flatter, implying that the outflow has the effect of reddening the observed spectrum. Recently, Baskin et al. (2013) used the mean SDSS spectra constructed by selecting on various QSO properties to investigate the outflow dependence on those properties. They found that the BAL-trough becomes deeper for QSOs with low He II $\lambda 1640$ Å EW or flatter UV slope. Our result is consistent with theirs. The intrinsic dust Small-Magellanic-Cloud-like (SMC-like) reddening in QSO spectra is discussed in some studies (e.g. Baskin et al. 2013). For this single BAL QSO, the larger BAL-trough EW with flatter spectrum implies an important role for the ionizing continuum in the trough variation.

The origin of BALs is commonly thought to be the result of subtending a disk wind in the line of sight. The disk wind may be subject to different physical effects in different zones of its outflow velocity structure. It was found that the high-velocity components of the C IV BAL-trough change much more than the low-velocity part with the change of He II $\lambda 1640$ Å EW, which is a measurement of the extreme

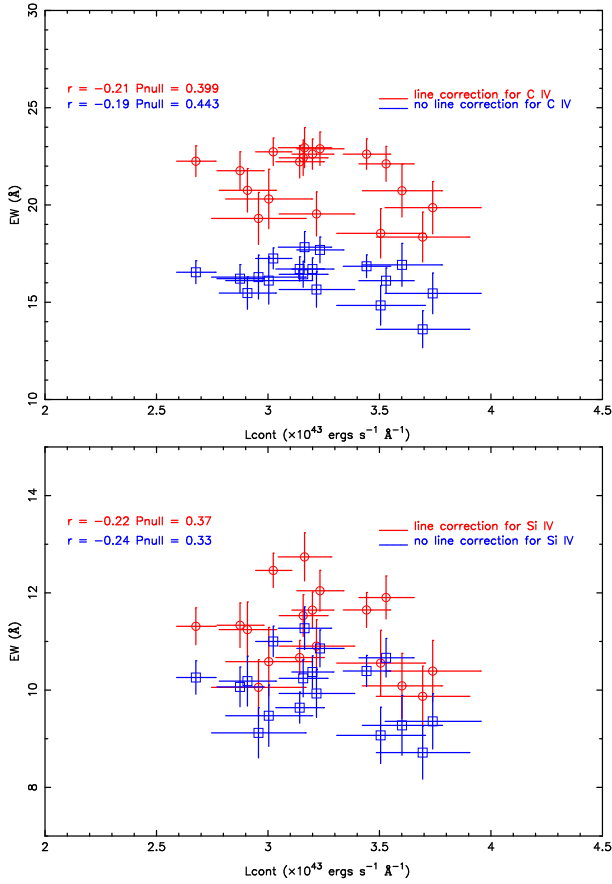


Figure 8. The EW versus the continuum luminosity for the C IV BAL (top), and for the Si IV BAL (bottom). The symbols are the same as in Fig. 7.

UV continuum (Baskin et al. 2013). Here we divide the total trough EW into two parts, for high-velocity and low-velocity. For the C IV BAL-trough, the wavelength range is between 1450 Å and 1500 Å ($\sim 20000 \text{ km s}^{-1} - 10000 \text{ km s}^{-1}$) for the high-velocity part, and between 1500 Å and 1549 Å ($\sim 10000 \text{ km s}^{-1} - 0 \text{ km s}^{-1}$) for the low-velocity part. For the Si IV BAL-trough, the wavelength range is between 1340 Å and 1355 Å ($\sim 13000 \text{ km s}^{-1} - 9700 \text{ km s}^{-1}$) for the high-velocity part, and between 1355 Å and 1400 Å ($\sim 9700 \text{ km s}^{-1} - 0 \text{ km s}^{-1}$) for the low-velocity part.

For the C IV BAL, the Spearman coefficients for the correlation between the divided BAL-trough EWs and the spectral index α are 0.64 (0.0042) for the high velocity part and 0.87 (0.000003) for the low-velocity part. The Spearman correlation coefficients are 0.75 (0.0003) for the high-velocity part of the Si IV BAL and 0.82 (0.00003) for the low-velocity part, where the values in brackets are the probabilities of the null hypothesis. It seems that the correlation between the spectral index and EW for the low-velocity part is slightly stronger than that for the high-velocity part. That result is consistent with the study of (Zhang et al. 2014), where they found that the UV slope affects the low-velocity part of outflows much more.

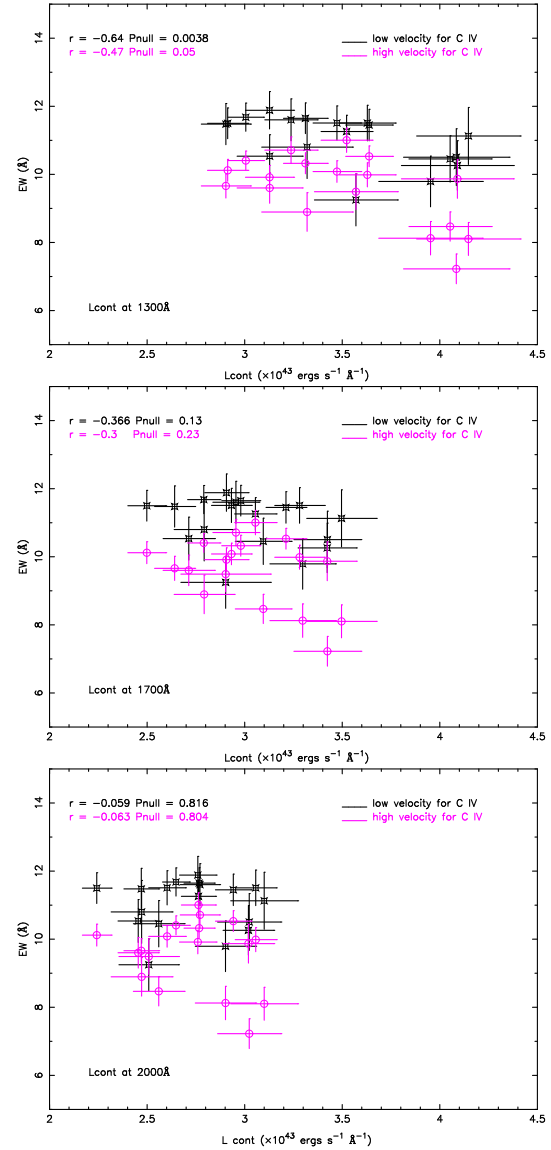


Figure 9. C IV BAL EW vs the continuum, where the continuum luminosity is measured at 1300 Å (top), at 1700 Å (middle) and 2000 Å (bottom), respectively. The black star is for the low-velocity part of the BAL-trough and the pink circle is for the high-velocity part of the BAL-trough.

4.5 EW versus the continuum

The dependence of the EW variability on QSO properties, such as the continuum luminosity, is still a question for debate (e.g., Gibson 2008; Filiz Ak et al. 2013; Baskin et al. 2013). Fig. 8 displays the correlation between BAL-trough EW and the continuum luminosity for C IV (top panel) and Si IV (bottom panel). As in Fig. 7, blue squares denote the EW_1 data and red circles denote the EW_2 data. The correlation between the EW and the continuum is weak. The Spearman coefficient is -0.19 (0.443) for C IV EW_1 , -0.21 (0.399) for C IV EW_2 , -0.24 (0.33) for Si IV EW_1 , and -0.22 (0.37) for EW_2 , where the values in brackets are the probabilities of the null hypothesis. The correlation between EW and the continuum is weak with a large probability of the null hypothesis. There is no significant correlation found in this

QSO. It is consistent with the study of Filiz Ak et al. (2013) who found no significant evidence for EW variability of C IV BAL-trough driven by the QSOs bolometric luminosity. We also calculated the Spearman coefficients between EW and the continuum for the high-velocity and low-velocity parts separately. The correlation coefficient between EW and the continuum is about -0.22 (0.39) (high-velocity) and -0.28 (0.26) (low-velocity) for the C IV BAL-trough, and is -0.35 (0.15) (high-velocity) and -0.22 (0.39) (low-velocity) for the Si IV BAL-trough, where the values in brackets are the probabilities of the null hypothesis. There is still no significant correlation between EW and the continuum for either the high-velocity or low-velocity parts.

We also measured the continuum luminosity at 1300 Å, 1700 Å, 2000 Å, respectively (Fig. 9). The Spearman correlation coefficient between EW and the continuum luminosity (1300 Å) for the C IV BAL is about -0.64 (0.0038) (low-velocity) and -0.47 (0.05) (high-velocity). For the continuum at 1700 Å, the correlation coefficient is -0.366 (0.13) (low-velocity) and -0.3 (0.23) (high-velocity). For the continuum at 2000 Å, the correlation coefficient is -0.059 (0.816) (low-velocity) and -0.063 (0.804) (high-velocity). The values in brackets are the probabilities of the null hypothesis. We find that the correlation becomes stronger when the continuum luminosity is measured in the bluer bands. The measured continuum luminosity in the bluer bands is more affected by dust extinction. This result is consistent with the correlation between the BAL-trough EW and the spectral index.

4.6 The maximum velocity of outflow

The C IV maximum velocity of outflow V_{max} for the 18 observations changed by about 10% (Table 2). In Fig. 10, we show the relation between V_{max} and the spectral index α . There is a moderately strong correlation between them with Spearman coefficient of 0.63 ($P_{null} = 0.0005$). This moderately strong correlation suggests larger extinction for larger maximum velocity of outflow. As we find a strong correlation between the BAL-trough EW and the spectral index, there should be a correlation between V_{max} and the C IV BAL-trough EW, and indeed, the Spearman coefficient is 0.78 ($P_{null} = 0.00013$). For flatter UV slope and the correspondingly larger BAL-trough, V_{max} becomes larger. For the correlation between V_{max} and the continuum (measured from 1300 Å to 2400 Å), the Spearman coefficient is -0.33 ($P_{null} = 0.174$). A weak negative correlation seems to exist between V_{max} and the continuum with a probability of 82.6%. The weak negative correlation between V_{max} and the luminosity for this one QSO is not consistent with the positive correlation found by others (e.g. Laor & Brandt 2002). However, we should note that our correlation between V_{max} and the luminosity is weak. More data are needed in the future for this study.

5 SUMMARY

The variability of the broad absorption lines is investigated for a broad absorption line QSO, SDSS J022844.09+000217.0 ($z = 2.719$), with 18 SDSS/BOSS

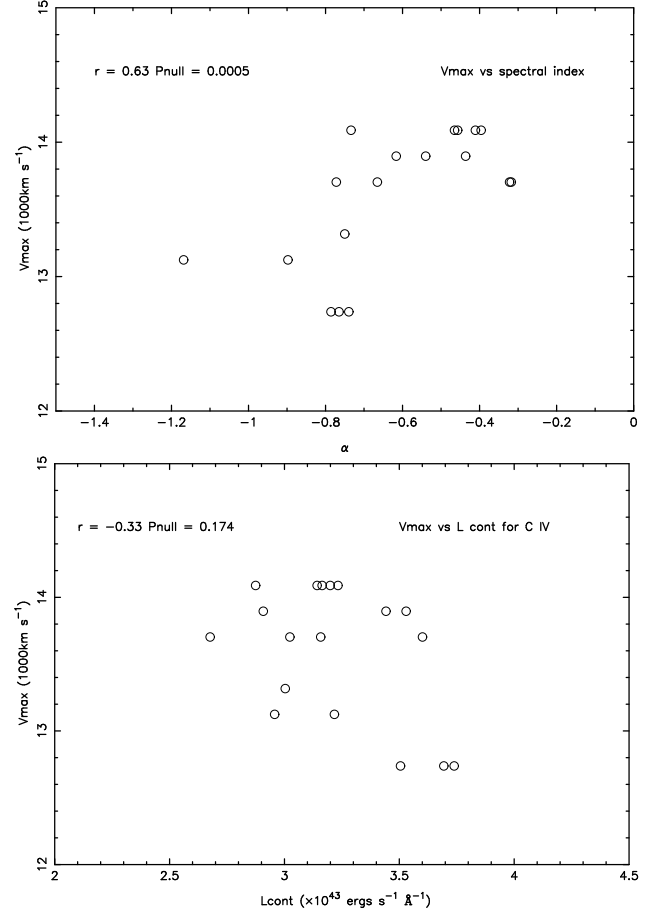


Figure 10. The maximum velocity of outflow versus spectral index α and the continuum (measured from 1300 Å to 2400 Å). The Spearman correlation coefficient for the maximum velocity and spectral index α is 0.63 with $P_{null} = 0.0005$. The Spearman correlation coefficient for the maximum velocity and the continuum is -0.33 with $P_{null} = 0.174$.

spectra covering 4128 days in the observational frame. The main conclusions can be summarized as follows:

- (1) The light curves for the BAL C IV EW, the continuum, and the spectral index are given. The EW for the C IV BAL-trough changes by about 25% (from 18.1 Å to 22.9 Å). The α changes by about 260% (from -0.32 to -1.16). The continuum luminosity changes by about 38% (from 2.67 to 3.69, in units of $10^{43} \text{ erg s}^{-1} \text{ Å}^{-1}$).
- (2) Through the rms-to-mean ratio spectrum, the relative flux change increases as the frequency increases, from about 10% on the red side, to about 15% on the blue side. The fractional variability is larger for the absorption trough than for the continuum and the emission lines.
- (3) There is a strong positive correlation between the C IV BAL-trough EW and UV spectral index α , as well as for the Si IV BAL-trough. The larger BAL-trough EW with flatter spectrum implies that the outflow has the effect of reddening the observed spectrum. The Spearman coefficient between the spectral index and BAL-trough EW for the low-velocity part is slightly larger than that for the high-velocity part. The strong correlation between the BAL-trough EW and the spectral index for this one QSO suggests that dust is intrinsic to outflows.

(4) There is no significant correlation between the C IV BAL-trough EW and the continuum in this QSO, nor for the Si IV BAL-trough. We do not find significant evidence for EW variability of the C IV BAL-trough driven by the QSO's bolometric luminosity. We find that the correlation becomes stronger when the continuum luminosity is measured in the bluer bands. The weak correlation between the BAL variability and the continuum luminosity for this one QSO implies that the BAL-trough variation is not dominated by photoionization.

(5) There is a moderately strong correlation between the maximum velocity of the C IV BAL-trough and the spectral index α for this QSO. However, there is no significant correlation between the maximum velocity of outflow and the continuum. More observations are needed in the future for this study.

6 ACKNOWLEDGMENTS

We are very grateful to the anonymous referee for her/his instructive comments which significantly improved the content of the paper. We thank Richard Green F. very much for the grammar-correction and comments in the paper. This work has been supported by the National Science Foundations of China (No. 11373024; 11173016; 11233003).

REFERENCES

- Allen J. T., et al. 2011, MNRAS, 410, 860
 Barlow T. A., Junkkarinen V. T., & Burbidge E. M. 1989, ApJ, 347, 674
 Barlow T. A., Junkkarinen V. T., Burbidge E. M., et al. 1992, ApJ, 397, 81
 Baskin A., Laor A., & Hamann F. 2013, MNRAS, 432, 1525
 Becker R. H., White R. L., Gregg M.D., Brotherton M.S., Laurent-Muehleisen S.A. & Arav N., 2000, ApJ, 538, 72
 Bian W. H., et al., 2012, ApJ, 759, 88
 Bruni G., et al., 2012, A&A, astro-ph/1203.4509
 Capellupo D. M., et al., 2011, MNRAS, 413, 908
 Capellupo D. M., et al., 2012, MNRAS, 422, 3249
 Capellupo D. M., et al., 2013, MNRAS, 429, 1872
 Cardelli J. A., Clayton G. C., & Mathis J. S., 1989, ApJ, 345, 245
 DiPompeo M. A., et al., 2012, MNRAS, 427, 1135
 Elvis M., 2000, ApJ, 545, 63
 Eisenstein D. J., et al., 2011, AJ, 142, 72
 Fabian A. C., 2012, ARA&A, 50, 455
 Filiz Ak, N., et al., 2012, ApJ, 757, 114
 Filiz Ak, N., et al., 2013, ApJ, astro-ph/1309.5364
 Fine S., Jarvis M.J., & Mauch T., 2011, MNRAS, 412, 213
 Forster K., et al., 2001, ApJS, 134, 35
 Ganguly R., Brotherton M. S., Cales S., et al. 2007, ApJ, 665, 990
 Ghosh K.K. & Punsly, B., 2007, ApJ, 661, L139
 Gibson R. R., et al., 2008, ApJ, 675, 985
 Gibson R. R., et al., 2009, ApJ, 692, 758
 Gregg M. D., Becker R. H., & de Vries W. 2006, ApJ, 641, 210
 Hall P. B., et al., 2002, ApJS, 141, 267
 Hewett P. C., & Foltz, C. B., 2003, AJ, 125, 1784
 Hu C., Wang J. M., Ho L. C., Chen Y. M., Zhang H. T., Bian, W. H., Xue, S. J., 2008, ApJ, 687, 78
 Kaspi S., Smith P.S., Netzer H., Maoz D., Jannuzi B.T., Giveon U., 2000, ApJ, 533, 631
 Laor, A., & Brandt, W. N., 2002, ApJ, 569, 64
 Lundgren B. F., Willite B. C., Brunner R. J., et al., 2007, ApJ, 656, 73
 Montenegro-Montes F. M., et al., 2008, MNRAS, 388, 1853
 Murray N., Chiang J., Grossman S. A., & Voit G. M., 1995, ApJ, 451, 498
 O'Donnell J. E., 1994, ApJ, 422, 158
 Paris I., Petitjean P., Aubourg E., et al., 2013, A&A, arXiv:1311.4870
 Proga D., Stone J. M., & Kallman T. R., 2000, ApJ, 543, 686
 Pu X. T., Bian W. H., & Huang K. L., 2006, MNRAS, 372, 24
 Shen Y., et al., 2011, ApJS, 194, 45
 Trump J. R., et al., 2006, ApJS, 165, 1
 Urry C. M., & Padovani P., 1995, PASP, 107, 803
 Vanden Berk D. E., Richards G. T., Bauer A., et al., 2001, AJ, 122, 54
 Voit G. M., Weymann R. J., & Korista K. T., 1993, ApJ, 413, 95
 Weymann R. J., Morris S. L., Foltz C. B., & Hewett P. C., 1991, ApJ, 373, 23
 Zhang S. H., et al., 2010, ApJ, 714, 367
 Zhang S. H., et al., 2014, ApJ, arXiv:1403.3166
 Zhou H., Wang T., Wang H., Wang J., Yuan W. & Lu Y., 2006, ApJ, 639, 716
 Zubovas K., & King, A., 2013, ApJ, 769, 51, arXiv:1304.1691